Research Article | Vol. 27, No. 20 / 30 September 2019 / Optics Express 27546

Optics EXPRESS

Experimental study on hybrid compensation testing of an off-axis convex ellipsoid surface

LISONG YAN,[1] DEYAN ZHU,[2] XUEFENG ZENG,[3] MING LI,[4] XIAOKUN WANG,[3] AND DONGLIN MA[1,*]

[1] *School of Optical and Electronic Information and Wuhan National Laboratory for Optoelectronics, Huazhong University of Science and Technology, Wuhan 430074, China*
[2] *Nanjing University of Aeronautics and Astronautics, Nanjing, Jiangsu 210000, China*
[3] *Key Laboratory of Optical System Advanced Manufacturing Technology, Changchun Institute of Optics, Fine Mechanics and Physics, Chinese Academy of Sciences, Changchun 130033, China*
[4] *Intane Optics, Nanjing 210046, China*
[*] *madonglin@hust.edu.cn*

Abstract: Aspherical surfaces can provide significant benefits to a wide variety of optical systems, but manufacturing high-precision aspherical surfaces has historically been limited by the ability to measure them. Null testing has always been the ideal method in aspherical measurement. However, in many cases, it is hard to realize null testing for complex surfaces, especially for convex surfaces in complicated forms. In this paper, we propose a hybrid compensation method combining a spherical mirror and a computer generated hologram (CGH) to achieve the null testing of the convex aspherical surface. Firstly, we introduce our self-developed mathematical models in the hybrid compensation method, including optics alignment model, distortion correction model and spherical surface error removing model. Then the performance of our proposed method is analyzed by a null testing experiment of an off-axis convex ellipsoid mirror. The experimental result shows that the proposed method can accomplish the hybrid compensation testing of convex aspherical surfaces effectively, and it can also bring much to the application of our method in convex aspherical surface testing.

1. Introduction

It is well known that measuring large convex aspherical surfaces is difficult because the required aperture of the auxiliary optics used in the testing is significantly larger than the optics being tested [1].

In this case, subaperture stitching testing is developed to overcome the aperture size limitations of conventional interferometry and the difficulty of acquiring auxiliary optics in large aperture [2]. The stitching technique has been studied by many scholars [3–16] and relative subaperture stitching interferometer (SSI) has also been developed by QED [17]. However, as the departure of an asphere from its best-fit sphere increases, the fringe densities within each subaperture increase. The increase can result in smaller measurable regions, and thereby require more subapertures for the testing, which might invalidate the subaperture stitching method. To solve the issue, QED introduced variable null optics (VON) method to drastically reduce the fringe density in subapertures [18,19], and thereby to reduce the number of subapertures required as well as enlarging the measurement ability. In this method, subapertures are non-null tested and retrace error [20,21] should be considered for each subaperture testing data, which makes the stitching complicated. A few large convex mirrors, both spherical and aspherical, have also been tested at the University of Arizona [22]. For example, they combined elements of the holographic test plate, subaperture Fizeau testing with an aspheric reference, and use of a computer generated hologram (CGH) to compensate the Fizeau testing with a spherical reference to achieve the testing of the secondary mirror of Large Synoptic Survey Telescope (LSST) [23].

#373116 https://doi.org/10.1364/OE.27.027546
Journal © 2019 Received 18 Jul 2019; revised 15 Aug 2019; accepted 3 Sep 2019; published 16 Sep 2019

In this paper, we propose a hybrid compensation method combining a spherical mirror and a CGH to accomplish the null testing of the convex aspherical mirror. Commercial interferometer is adopted in the testing and only four optics (interferometer, CGH, spherical mirror, aspherical mirror tested) are placed in the testing path, which makes the structure of the optical path simple. The spherical mirror with a relatively large aperture is relatively easy to fabricate. Meanwhile, we can also easily get the access to the CGH due to its non-tight processing requirements. Our proposed method provides an efficient way to accomplish the null testing of convex aspherical mirrors, especially for high-departure aspheres. Spherical mirror in our method can help compensate for some part of aberrations such as astigmatism and coma, and the residual aberrations can be compensated by CGH because of its flexibility in design. The paper is organized as follows. In Section 2, the basic theory of hybrid compensation is introduced. In Section 3, we apply the proposed method to the actual experiment and the relative testing result is analyzed. The conclusion is given in Section 4.

2. Theory

In this part, the design concept of hybrid compensation testing including the structure of testing path and alignment methods between every optical element are described in section 2.1. Then the relative data processing and error analysis are studied in section 2.2.

2.1. *Design concept of hybrid compensation testing*

2.1.1. Structure of optical path

The convex aspherical surface can be tested in full aperture with hybrid compensation method combining a spherical mirror with a CGH as shown in Fig. 1. The aberrations introduced in the off-axis aspherical surface testing mainly include astigmatism and coma, which can be compensated with a spherical mirror and a CGH. During the testing, a spherical mirror with relatively large aperture is adopted to provide a convergent wavefront. The spherical mirror also compensates some part of astigmatism and coma in the testing, while the residual of the aberrations is completely compensated with the CGH.

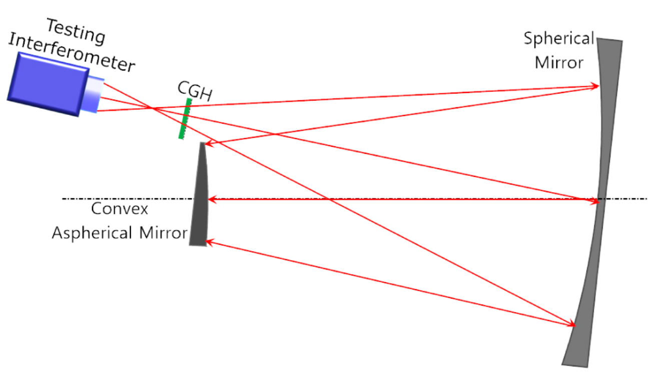

Fig. 1. Hybrid compensation with CGH and spherical mirror.

2.1.2. Alignment design of optics

Since there are four components in the optical path, the non-alignment among them will introduce extra aberrations in the testing map, which will cause the testing map to be non-consistent with the actual surface map. As a result, alignment of each optical component should be taken accurately in the testing.

Accurate optics alignment is achieved by designing alignment regions on the CGH directly. To accomplish the alignment between optics and the testing of aspherical mirror, five kinds of diffractive region shown in Table 1 can be designed on CGH.

Table 1. Summary of CGH regions

Region number	Function of the region
Region 1	Compensation region: Realize the compensation of aspherical wavefront
Region 2	Alignment region: Accomplish the alignment between CGH and alignment interferometer
Region 3	Alignment region: Accomplish the alignment between CGH and testing interferometer
Region 4	Alignment marks projected region: project cross line around the spherical mirror
Region 5	Alignment marks projected region: project cross line around the aspherical mirror

Based on the regions described in Table 1, the alignment of optics can be achieved according to the following steps.

Step 1: Accomplish the null testing of the spherical mirror with an auxiliary alignment interferometer as shown in Fig. 2. After the step, two components including the spherical mirror and the alignment interferometer are in the optical path and they are aligned accurately.

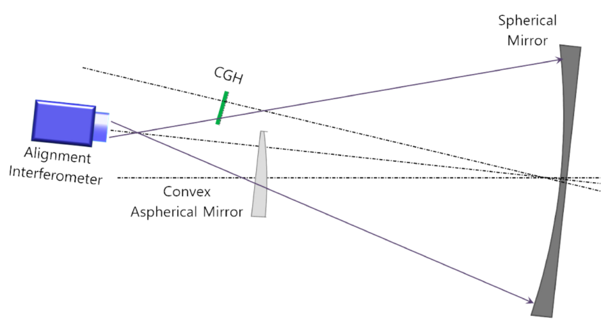

Fig. 2. Alignment process (step1 and step2)

Step 2: Put CGH in the optical path as shown in Fig. 2. Adjust the position of the CGH according to the interferogram formed by region 2 on CGH until null testing is attained. After this step, three components including the spherical mirror, the alignment interferometer and the CGH have been accurately aligned in the optical path.

Step 3: Place the testing interferometer into the optical path as shown in Fig. 3. Adjust the position of the testing interferometer according to the interferogram formed by region 3 on CGH until null testing is attained. Now the alignment between testing interferometer, the CGH and the spherical mirror is fulfilled. At the same time, cross lines (formed by region 4 on the CGH) can be observed around the spherical mirror.

Step 4: Lay the aspherical mirror into the optical path according to the cross lines (formed by region 5 on the CGH) projected around the aspherical mirror as shown in Fig. 3. Then interferogram of the aspherical mirror testing will be obtained (formed by region 1 on the CGH). Adjust the position of the aspherical mirror according to the interferogram until the alignment between four components including testing interferometer, CGH, spherical mirror and the aspherical mirror are well done.

In the alignment process as shown in Fig. 2 and Fig. 3, two interferometers including testing interferometer and alignment interferometer are introduced at the same time. The advantage of introducing the alignment interferometer is that it can be used to ensure that the spherical mirror is aligned with CGH during testing.

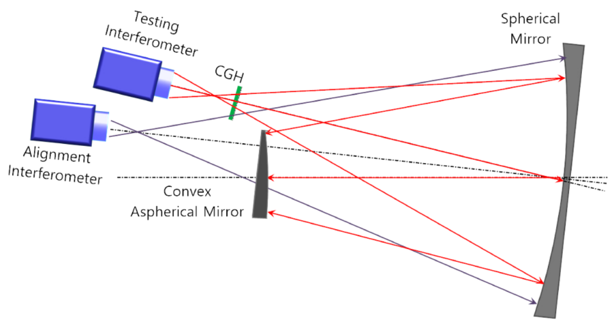

Fig. 3. Alignment process (step3 and step4)

2.2. Data processing and error analysis

In this part, we mainly discuss two problems including distortion correction and removal of spherical mirror surface error in the surface map of aspherical mirror. To better explain these two problems, we first define the following coordinate systems as shown in Fig. 4 and Fig. 5.

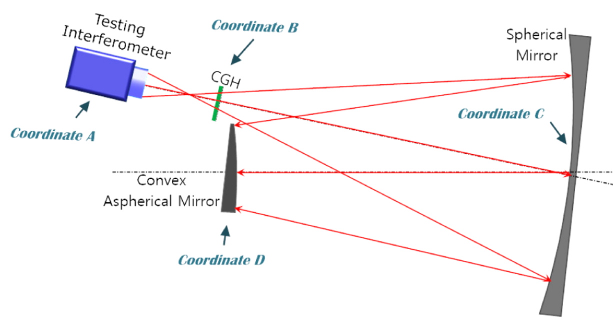

Fig. 4. Description of coordinate systems in testing

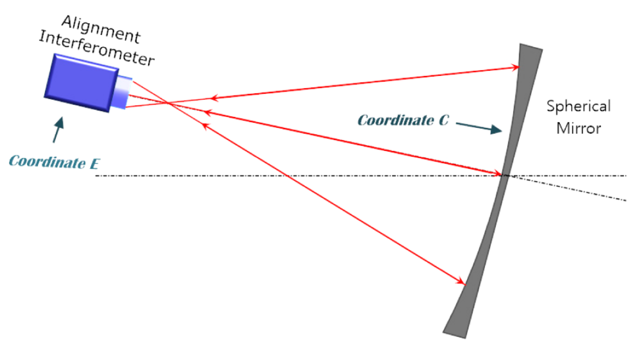

Fig. 5. Description of coordinate systems in alignment

After accomplishing the alignment between optical elements in the optical path as shown in Fig. 4, we define the coordinate of the testing interferometer as coordinate A; the coordinate of CGH plane as coordinate B; the coordinate of spherical mirror surface as coordinate C; the coordinate of convex aspherical mirror surface as coordinate D. Before the testing of aspherical surface, the spherical mirror was accurately aligned and tested with alignment interferometer as shown in Fig. 5 (this step is described in step 1 in section 2.1.2). The coordinate of alignment interferometer is defined as coordinate E.

2.2.1. Distortion correction

Distortion will be introduced in the hybrid compensation testing of the aspherical mirror, and cause the inconsistency between the area shape of interferogram and the actual physical shape. It should be corrected before the follow-up processing applied to the mirror.

Distortion correction can be taken with targets, which have been affixed on surfaces of both the spherical mirror and the aspherical mirror respectively before testing. Usually four targets are needed to paste on the spherical mirror, while another four targets are needed to paste on the aspherical mirror. In order to achieve the distortion correction in high-accuracy, we provided a correction model based on ray tracing and affine transformation. The correction model can be separated into two parts. Firstly, the nonlinear transformation is taken between coordinate systems of CGH and convex aspherical surface by ray tracing. Secondly, the linear transformation is taken between the coordinate systems of testing interferometer and CGH with target points whose position coordinates can be tested accurately.

A. Coordination relationship from CGH to testing surface The relationship between CGH to testing surface can be obtained by ray tracing. Tracking points can be set on testing surface as shown in Fig. 6(a) and uniformed grid rays are ejected along the normal direction of the testing surface. The relative positions of tracking points on CGH plane according to the experimental parameters as described in section 3 are shown in Fig. 6(b) as expressed with intersection points. Therefore, according to the ray tracing method, the coordinate relationship can be established between coordinate D and coordinate B as shown in Fig. 4.

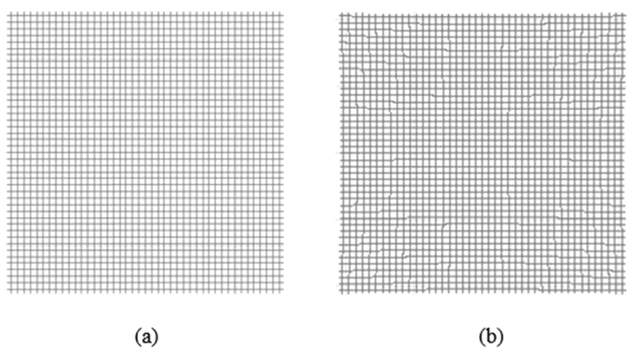

Fig. 6. Distortion of a convex aspherical mirror with hybrid compensation: (a) uniform grid on the aspherical mirror on the test, (b) uniform grid mapping to the CGH

B. Coordinate relationship from CCD to CGH The coordinate relationship from CGH to testing surface was obtained with ray tracing method, while the coordinate relationship from testing interferometer CCD to CGH was established based on affine transformation.

In the distortion correction, the coordinates of targets in the testing interferometer results can be described as $(x_i,\ y_i), i = 1, 2, 3, \ldots$, while the relative coordinates in the CGH plane can be written as $(X_i,\ Y_i),\ i = 1, 2, 3, \ldots$. Based on the theory of affine transformation, the relationship

Optics EXPRESS

between them should be as follows:

$$\begin{bmatrix} X_i \\ Y_i \\ 1 \end{bmatrix} = T \cdot \begin{bmatrix} x \\ y \\ 1 \end{bmatrix}, \tag{1}$$

where

$$T = \begin{bmatrix} s \cdot \cos\theta & -s \cdot \sin\theta & t_x \\ s \cdot \sin\theta & s \cdot \cos\theta & t_y \\ 0 & 0 & 1 \end{bmatrix}, \tag{2}$$

where s is the magnification of each pixel in the CCD testing result, (t_x, t_y) is the relative translation between the coordinates of CCD and CGH plane, and θ is the relative rotation degree between them. In the coordinate relationship from CCD plane to CGH plane, s should be the same to every point.

Then the relationship between the CCD testing coordinates before and after the affine transformation should be:

$$\begin{bmatrix} X_i' \\ Y_i' \end{bmatrix} = \begin{bmatrix} x_i \cdot s \cdot \cos\theta - y_i \cdot s \cdot \sin\theta + t_x \\ x_i \cdot s \cdot \sin\theta + y_i \cdot s \cdot \cos\theta + t_y \end{bmatrix}, \tag{3}$$

where $(X_i',\ Y_i')$ is the coordinate of pixel $(x_i,\ y_i)$ after affine transformation. By minimizing the sum,

$$\min = \sum_{i=1}^{N} ((X_i' - X_i)^2 + (Y_i' - Y_i)^2), \tag{4}$$

where N is the number of targets, matrix T can be solved and the coordinate relationship from CCD plane to CGH plane can be obtained, which means coordinate relationship can be established between coordinate A and coordinate B as shown in Fig. 4.

With the above two processes of A and B, the coordinate relationship between coordinate A and D as shown in Fig. 4 is achieved, which means that the point-to-point correspondence between the aspherical surface and testing interferometer has been found, and the distortion correction of testing map can be accomplished.

2.2.2. Removal of spherical mirror surface error

In the hybrid compensation testing, the surface error of spherical mirror in Fig. 4 will be introduced into the testing map as a system error, which makes the testing map different from the actual surface map of the aspherical surface. The surface map of spherical mirror should also be removed from testing map. Targets affixed on the spherical mirror surface before testing can be used to accomplish the spherical surface's error removal. The spherical surface's error removal model can also be separated into two parts.

Firstly, the spherical mirror is aligned and tested with alignment interferometer directly as shown in Fig. 5. In this process, the surface error of spherical mirror is obtained and the coordinate relationship between coordinate C and coordinate E is achieved as shown in Fig. 5.

Secondly, the coordination relationship from testing interferometer to spherical surface in the convex aspherical surface testing path as shown in Fig. 4 can be obtained with the theory described in section 2.2.1. Actually, the coordinate relationship between coordinate A and coordinate B can be derived with affine transformation theory, while the coordinate relationship

Optics EXPRESS

between coordinate B and coordinate C can be found with ray tracing method. Therefore, the coordinate relationship between coordinate A and coordinate C is established.

From what has been discussed above, the coordinate relationship between coordinate A and coordinate E can be achieved, which means that the spherical surface error (testing map in coordinate E as shown in Fig. 5) can be removed from the aspherical testing map (testing map in coordinate A as shown in Fig. 4). Therefore, the removal of spherical mirror surface error is accomplished.

3. Experiment verification

In this experiment, the aperture of the off-axis convex ellipsoid mirror is 332mm×144mm. Conic constant κ is −0.54 and the vertex radius of curvature R is −933mm. The off-axis amount of the aspherical mirror is 86.2mm. The Peak-to-Valley (PV) and Root mean square (RMS) departure between the off-axis convex ellipsoid and the best-fit sphere is 132.4445λ and17.4936λ respectively as shown in Fig. 7.

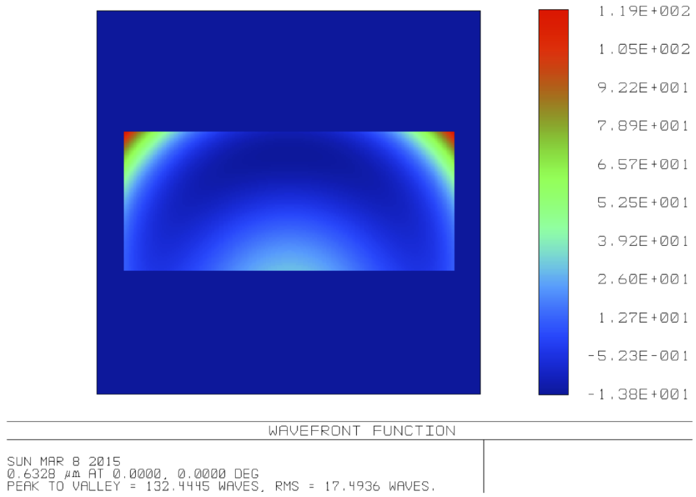

Fig. 7. Departure between ellipsoid mirror and best-fit sphere

To accomplish the full aperture testing of the off-axis convex ellipsoid mirror, a spherical mirror with 750mm aperture, 1550mm radius of curvature, and a CGH are introduced in the experiment. The design of testing path is shown in Fig. 8.

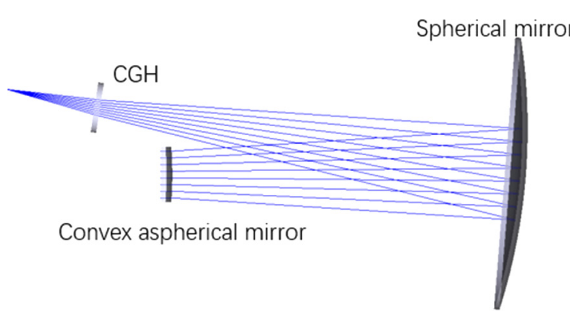

Fig. 8. Design of testing path

Optics EXPRESS

Part of the aberration is compensated by the spherical mirror surface and the rest of the residual error is compensated with the CGH. When light reflected from the spherical mirror, the new aberration is introduced into the optical path, which also compensated the departure between the off-axis convex ellipsoid and its best-fit sphere. The residual error after the compensation of the spherical mirror is shown in Fig. 9. It can be seen from Fig. 7 and Fig. 9 that the aberrations form as well as their magnitude are in consistent, which means that the spherical mirror compensates part of the aberration.

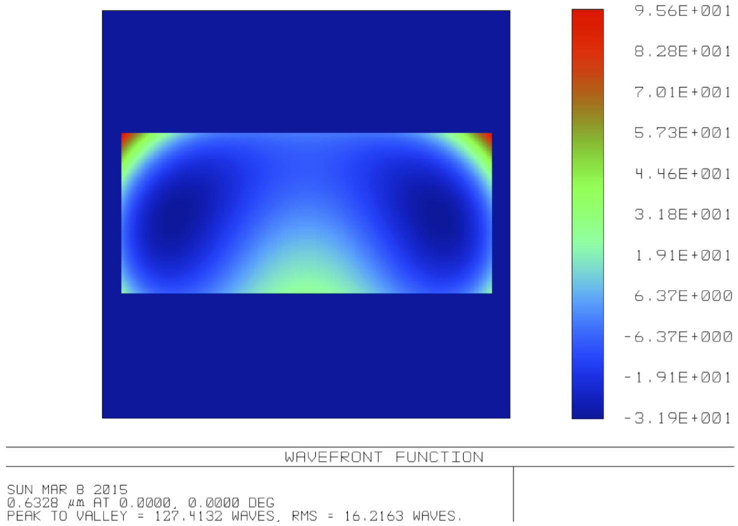

Fig. 9. Residual error after compensated with spherical mirror

Then the rest of the aberration is compensated with the CGH, and the residual error after the compensation of the CGH can be acquired as shown in Fig. 10.

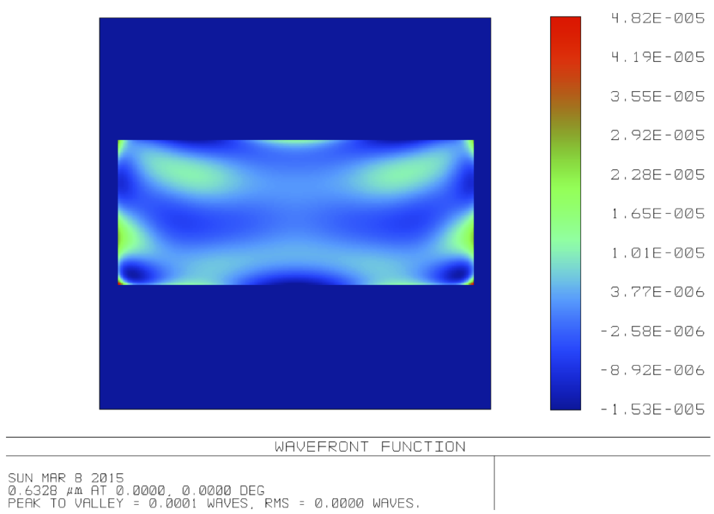

Fig. 10. Residual error after CGH compensation

Optics EXPRESS

It can be seen from Fig. 10 that the PV and RMS residual in the design is 0.0001λ and 0 respectively, which means that the off-axis convex ellipsoid mirror can be tested with our method in full aperture with a high accuracy theoretically.

To accomplish the alignment between optics, five kinds of diffractive region are designed on CGH as shown in Fig. 11. The fabricated CGH used in the measurement is shown in Fig. 12.

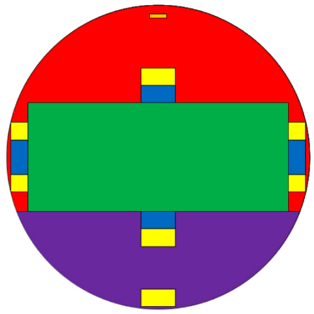

Fig. 11. Diffractive regions distribution on CGH

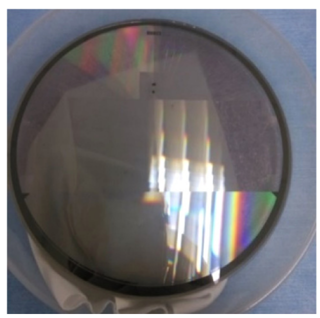

Fig. 12. CGH used in the measurement

The functions of each diffractive region shown in Fig. 11 are described in Table 2.

Table 2. Description of CGH regions

Region color	Function of the region
Green region	Compensation region: Realize the compensation of aspherical wavefront
Purple region	Alignment region: Accomplish the alignment between CGH and alignment interferometer
Red region	Alignment region: Accomplish the alignment between CGH and testing interferometer
Yellow region	Alignment marks projected region: project cross line around the spherical mirror
Blue region	Alignment marks projected region: project cross line around the aspherical mirror

Based on the regions described in Table 2, the alignment of optics shown in Fig. 13 can be achieved according to the following steps:

Step 1: Accomplish the null testing of the spherical mirror with an auxiliary alignment interferometer. The interferograms before and after alignment are shown in Fig. 14. After the step, two components including the spherical mirror and the alignment interferometer are in the optical path and they are aligned accurately.

Step 2: Put CGH in the optical path and adjust the position of the CGH according to the interferogram formed by purple region shown in Fig. 11 on CGH until null testing is attained. The

Optics EXPRESS

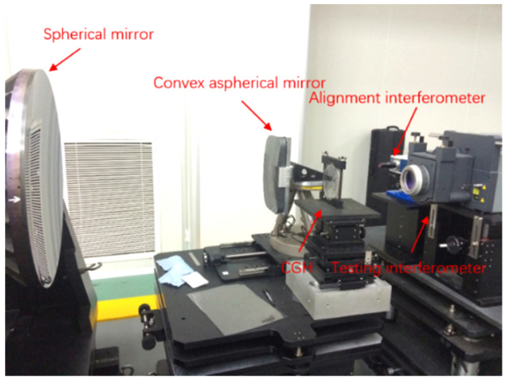

Fig. 13. Testing setup

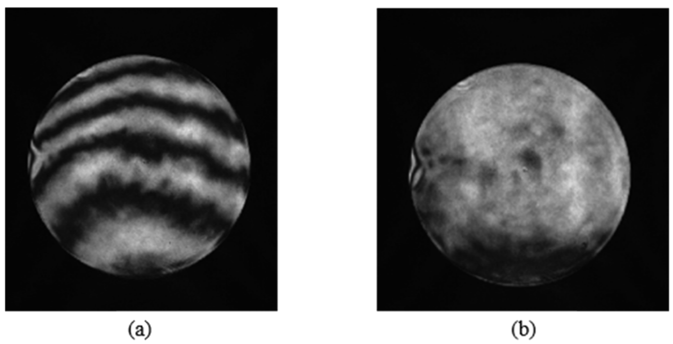

Fig. 14. Test sphere with alignment interferometer (a) Interferogram before alignment between spherical mirror and alignment interferometer (b) Interferogram after alignment between spherical mirror and alignment interferometer

interferograms before and after alignment are shown in Fig. 15. After this step, three components including the spherical mirror, the alignment interferometer and the CGH are accurately aligned in the optical path.

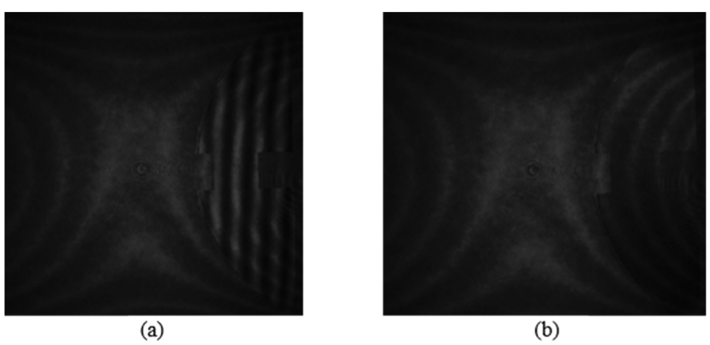

Fig. 15. Align CGH with alignment interferometer (a) Interferogram before alignment between spherical mirror, CGH and alignment interferometer (b) Interferogram after alignment between spherical mirror, CGH and alignment interferometer

Optics EXPRESS

Step 3: Place the testing interferometer into the optical path and adjust the position of the testing interferometer according to the interferogram formed by red region on CGH until null testing is attained. Now the alignment between testing interferometer, the CGH and the spherical mirror is fulfilled. The interferograms before and after alignment are shown in Fig. 16. At the same time, cross lines (formed by yellow region on the CGH) can be observed around the spherical mirror, which indicates the area of the spherical mirror used in the testing.

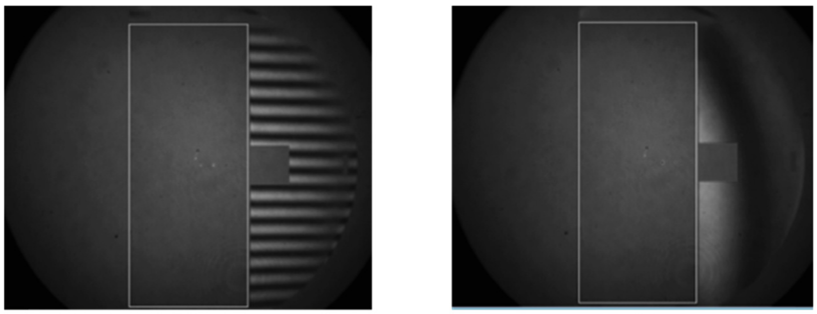

(a) (b)

Fig. 16. Align CGH with testing interferometer (a) Interferogram before alignment between spherical mirror, CGH and testing interferometer (b) Interferogram after alignment between spherical mirror, CGH and testing interferometer

Step 4: Lay the aspherical mirror into the optical path according to the cross lines (formed by blue region on the CGH) projected around the aspherical mirror. Then interferogram of the aspherical mirror testing will be obtained (formed by green region on the CGH). Adjust the position of the aspherical mirror according to the interferogram until the alignment between four components including testing interferometer, CGH, spherical mirror and the aspherical mirror are well done. The interferograms before and after alignment are shown in Fig. 17.

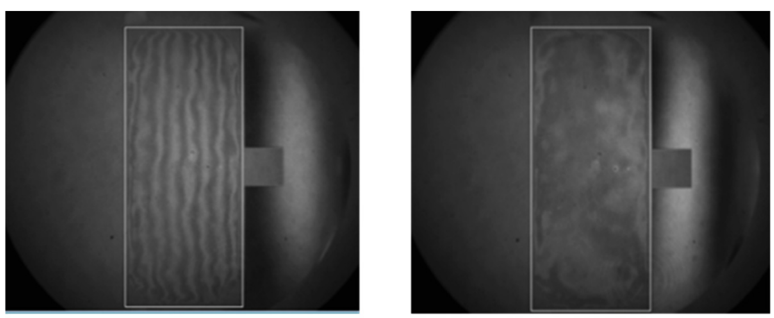

(a) (b)

Fig. 17. Align aspherical mirror (a) Interferogram before alignment between spherical mirror, CGH, testing interferometer and aspherical mirror (b) Interferogram after alignment between spherical mirror, CGH, testing interferometer and aspherical mirror

In the experiment, two interferometers including the alignment interferometer and tesing interferometer are introduced. The advantage of introducing the alignment interferometer is that it can be used to ensure that the spherical mirror is aligned with CGH during testing, which means no extra misalignment aberrations between them are introduced in the aspherical mirror testing result. After the above steps, the testing map of aspherical surface is shown in Fig. 18. For the black holes in Fig. 18, it is the pixels corresponding to the targets' locations in aspherical and

Optics EXPRESS

spherical mirrors. The relative testing map of spherical mirror can also be acquired in step 1 as shown in Fig. 19. As the spherical mirror are not used in full aperture in the hybrid compensation testing, the relative area used in the testing can be calculated with the theory described in section 2.2.2 with the targets marked on the surface of spherical mirror and aspherical mirror separately. The surface error of the above area is shown in Fig. 20. After distortion correction and removing the surface error of spherical mirror with the theory introduced in section 2.2, the surface map of aspherical mirror is shown in Fig. 21. By filling the phase values of pixels corresponding to the targets' positions with triangulation interpolation method in Fig. 21 [8], the relative surface map of aspherical mirror is shown in Fig. 22. It can be seen from Fig. 22 that the PV and RMS of the aspherical surface map is 0.978λ and 0.044λ (λ=632.8 nm) respectively.

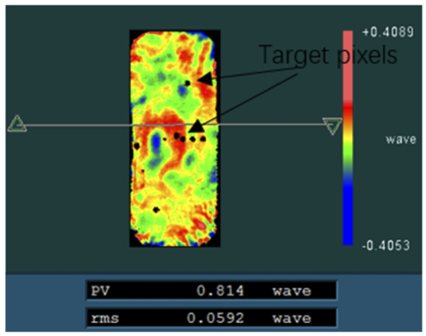

Fig. 18. Testing map of aspherical mirror

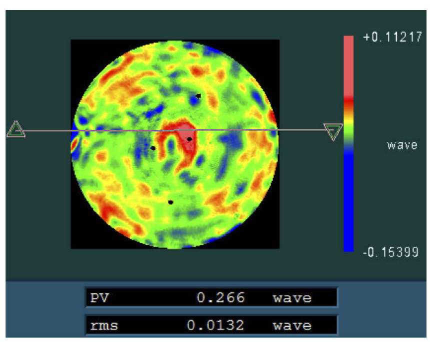

Fig. 19. Testing map of spherical mirror

For the purpose of cross test, eight different kinds of CGH in 150mm aperture respectively are designed and fabricated for the full aperture covering of the same off-axis convex ellipsoid mirror. The testing mirror is separated into eight subapertures as shown in Fig. 23. For each subaperture, it is null tested as shown in Fig. 24. The relative subaperture testing results are shown in Fig. 25. The validity and precision of our proposed method can then be verified by comparison with the null stitching testing results.

The PV and RMS of the aspherical surface map obtained by stitching testing is 0.956λ and 0.0419λ (λ=632.8 nm) respectively. By comparing Fig. 22 and Fig. 26, the surface map error obtained by proposed hybrid compensation testing is consistent with the null stitching testing result in the error distribution. Furthermore, both PV and RMS values achieved with the above two methods are comparable, which verifies the validity and precision of the proposed method.

Optics EXPRESS

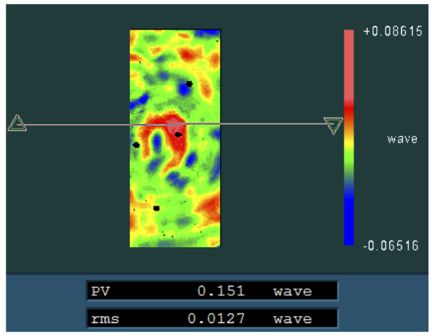

Fig. 20. Area of spherical mirror used in the hybrid compensation testing

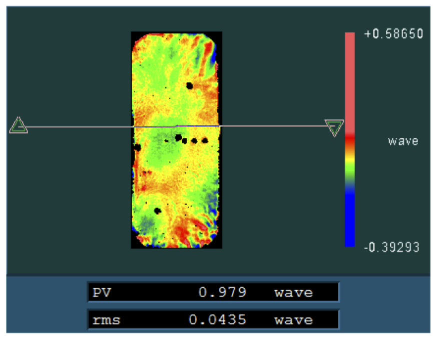

Fig. 21. Surface map of aspherical mirror after removing the error of spherical mirror

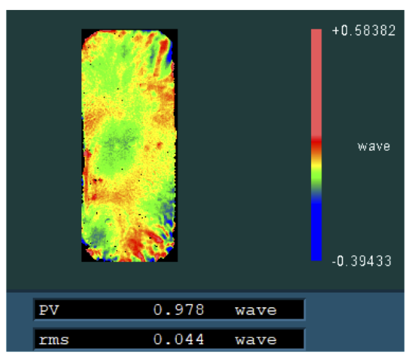

Fig. 22. Surface map of aspherical mirror after replacing the target pixels

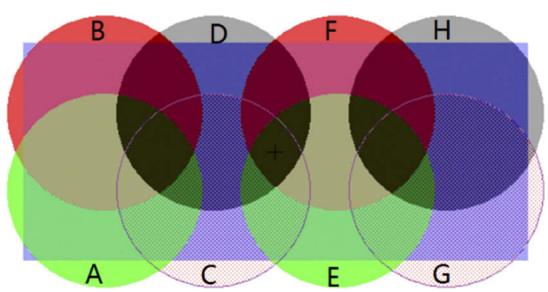

Fig. 23. Subapertures design with CGH

Optics EXPRESS

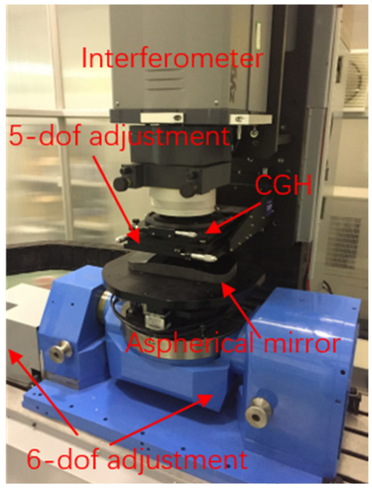

Fig. 24. The layout of subaperture testing system

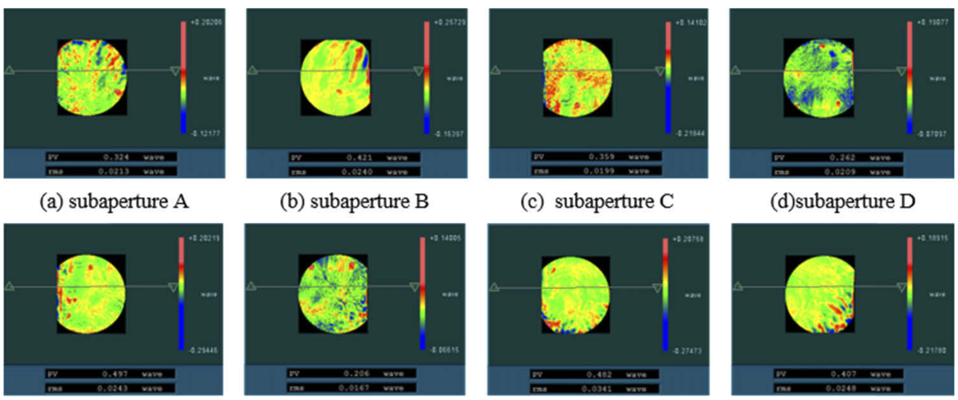

(a) subaperture A (b) subaperture B (c) subaperture C (d)subaperture D

(e) subaperture E (f) subaperture F (g) subaperture G (h) subaperture H

Fig. 25. Subaperture testing results

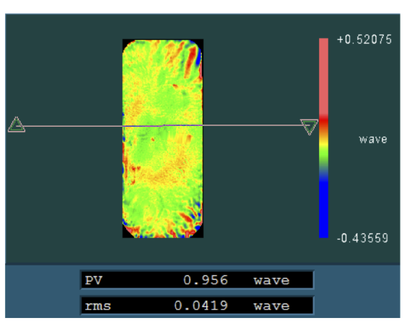

Fig. 26. Subaperture stitching map

Compared with the null stitching testing method, our proposed method in the paper possesses the following major advantages. Firstly, it overcomes the full aperture measurement limits for convex aspherical surface testing. With our method, the convex surface can be tested in full aperture by an interferometry, which avoids multiple measurements. Secondly, only one CGH is applied in our proposed method. It saves time and cost compared with the null stitching method, which needs eight different CGHs in our experiment. In general, our proposed hybrid compensation method can be an economical and fast test method in convex surface testing, especially for non-rotational symmetric convex surfaces in large aperture.

4. Conclusion

We have proposed a hybrid compensation method to measure convex aspherical surface in full aperture. With the above method, null testing can be accomplished. To avoid extra aberration caused by non-alignment between optics adding to the testing map, the accurate alignment between optics can be achieved with different diffractive regions on CGH. For a better testing accuracy, the surface error of spherical mirror is also removed. Distortion correction is finally taken to the testing map, which make the area shape of interferogram in consistent with the actual physical shape of the aspherical mirror, ensuring the feasibility of subsequent processing to the aspherical mirror. To evaluate the performance of our method, experiment verification is also taken. It can be proved from the above experiment result that the reported method can obtain the full-aperture surface map with satisfactory accuracy. As the experimental study is now for an off-axis aspherical mirror, further theoretical and experimental developments of the reported method on more complex surfaces such as freeform surfaces will be taken.

Funding

National Natural Science Foundation of China (61775067, 61805088, 61805089); Fundamental Research Funds for the Central Universities (2018KFYYXJJ053, 2019kfyRCPY083, 2019kfyXKJC040).

Acknowledgments

The authors would like to thank Chengli Guo from Sunny Optical technology, for his kind help in processing CGH in our experiment.

References

1. O. Masashi, O. Katsuyuki, and T. Jumper, "Measurement of large plane surface shapes by connecting small-aperture interferograms," Opt. Eng. **33**(2), 608–613 (1994).
2. C. J. Kim, "Polynomial fit of interferograms," Appl. Opt. **21**(24), 4521–4525 (1982).
3. Y. F. Wen, H. B. Cheng, H.-Y. Tam, and D. M. Zhou, "Modified stitching algorithm for annular subaperture stitching interferometry for aspheric surfaces," Appl. Opt. **52**(23), 5686–5694 (2013).
4. X. Hou, F. Wu, L. Yang, and Q. Chen, "Experimental study on measurement of aspheric surface shape with complementary annular subaperture interferometric method," Opt. Express **15**(20), 12890–12899 (2007).
5. Y. M. Liu, G. N. Lawrence, and C. L. Koliopoulos, "Subaperture testing of aspheres with annular zones," Appl. Opt. **27**(21), 4504–4513 (1988).
6. S. Y. Chen, S. Xue, Y. Y. Dai, and S. Y. Li, "Subaperture stitching test of large steep convex spheres," Opt. Express **23**(22), 29047–29058 (2015).
7. Z. X. Zhao, H. Zhao, F. F. Gu, H. B. Du, and K. X. Li, "Non-null testing for aspheric surfaces using elliptical sub-aperture stitching technique," Opt. Express **22**(5), 5512–5520 (2014).
8. L. S. Yan, X. K. Wang, L. G. Zheng, X. F. Zeng, H. X. Hu, and X. J. Zhang, "Experimental study on subaperture testing with iterative triangulation algorithm," Opt. Express **21**(19), 22628–22644 (2013).
9. L. Zhang, D. Liu, T. Shi, Y. Y. Yang, S. Y. Chong, B. L. Ge, Y. B. Shen, and J. Bai, "Aspheric subaperture stitching based on system modeling," Opt. Express **23**(15), 19176–19188 (2015).
10. S. Y. Chen, C. C. Wu, G. P. Tie, and D. D. Zhai, "Stitching test of large flats by using two orthogonally arranged wavefront interferometers," Appl. Opt. **56**(33), 9193–9198 (2017).

Optics EXPRESS

11. Q. Hao, S. P. Wang, Y. Hu, Y. F. Tan, T. F. Li, and S. S. Wang, "Two-step carrier-wave stitching method for aspheric and freeform surface measurement with a standard spherical interferometer," Appl. Opt. **57**(17), 4743–4750 (2018).
12. K. Nowick and K. Wagner, "Rannular subaperture interferometry for high-departure aspheres using paraboloidal parameterization," Appl. Opt. **58**(12), 3282–3292 (2019).
13. J. Z. Peng, D. F. Chen, H. W. Guo, J. G. Zhong, and Y. J. Yu, "Variable optical null based on a yawing CGH for measuring steep acylindrical surface," Opt. Express **26**(16), 20306–20318 (2018).
14. Y. C. Chen, C. W. Liang, H. S. Chang, and P. C. Lin, "Reconstruction of reference error in high overlapping density subaperture stitching interferometry," Opt. Express **26**(22), 29123–29133 (2018).
15. S. Xue, S. Y. Chen, and G. P. Tie, "Near-null interferometry using an aspheric null lens generating a broad range of variable spherical aberration for flexible test of aspheres," Opt. Express **26**(24), 31172–31189 (2018).
16. P. Su, J. H. Burge, and R. E. Parks, "Application of maximum likelihood reconstruction of subaperture data for measurement of large flat mirrors," Appl. Opt. **49**(1), 21–31 (2010).
17. P. Murphy, G. Forbes, J. Fleig, P. Dumas, and M. Tricard, "Stitching interferometry: a flexible solution for surface metrology," Opt. Photonics News **14**(5), 38–43 (2003).
18. A. Kulawiec, P. Murphy, and M.D. Marco, "Measurement of high-departure aspheres using subaperture stitching with the Variable Optical Null (VONTM)," Proc. SPIE **7655**, 765512 (2010).
19. C. Supranowitz, C.M. Fee, P. Murphy, G. Forbes, A. Kulawiec, and D. Miladinovic, "Asphere Metrology Using Variable Optical Null Technology," Proc. SPIE **8416**, 841604 (2012).
20. D. Liu, Y. Y. Yang, C. Tian, Y. J. Luo, and L. Wang, "Practical methods for retrace error correction in nonnull aspheric testing," Opt. Express **17**(9), 7025–7035 (2009).
21. C. Tian, Y. Y. Yang, T. Wei, and Y. M. Zhuo, "Nonnull interferometer simulation for aspheric testing based on ray tracing," Appl. Opt. **50**(20), 3559–3569 (2011).
22. J. H. Burge, "Fizeau interferometry for large convex surfaces," Proc. SPIE **2536**, 127–138 (1995).
23. M. B. Dubin, P. Su, and J. H. Burge, "Fizeau interferometer with spherical reference and CGH correction for measuring large convex aspheres," Proc. SPIE **7426**, 74260S (2009).